

Apoptosis of Multi-Drug Resistant *Candida* Species on Microstructured Titanium Surfaces

Phuc H. Le, Denver P. Linklater, Arturo Aburto-Medina, Shuai Nie, Nicholas A. Williamson, Russell J. Crawford, Shane Maclaughlin, and Elena P. Ivanova*

The proportion of hospital-acquired medical device infections caused by pathogenic, multi-drug resistant *Candida* species occurs in up to 10% of implantations. In this study, a unique antifungal micro-pillared titanium surface pattern is developed, which demonstrates both fungicidal and fungistatic activity, persistently deterring biofilm formation by *Candida albicans* and multi-drug resistant *Candida auris* fungi for up to 7 days. The Ti micropillars of 3.5 μm height are fabricated using maskless inductively coupled plasma reactive ion etching. The micro-textured surface consistently kills $\approx 50\%$ of *Candida* spp. irreversibly attached cells and prevent the proliferation of the remaining cells by inducing programmed cell death. Proteomic analysis reveals that *Candida* cells undergo extensive metabolic stress, preventing the transformation from yeast to the filamentous/hyphal cell phenotype that is essential for establishing a typical in vitro biofilm. The mechanical stress imparted following interaction with the micropillars injures attaching cells and induces apoptosis whereby the *Candida* cells are unable to be revived in a non-stress environment. These findings shed new insight toward the design of durable antifungal surfaces that prevent biofilm formation by pathogenic, multi-drug resistant yeasts.

infections have poor clinical outcomes corroborated by an associated high mortality rate.^[5] Indeed, candidemia is associated with a 15–35% attributable death rate in adults and a 10–15% mortality rate in newborns.^[6] *Candida* spp. are able to effectively colonize and form biofilms on implantable biomaterials. There is increasing concern for the implication of *Candida* spp. being involved in dental implant diseases as *Candida* are isolated in $\approx 30\%$ of peri-implantitis sites.^[7–9] Since the use of antifungal agents is not always effective in the case of infections caused by antifungal-resistant *Candida* spp., it is critical to develop alternative strategies for preventing their attachment and biofilm formation on implantable materials.

Within the last decade, it was determined that the nanostructured topographies observed on the surface of many insect wings could physically rupture bacterial cells.^[10–16] The nanostructured surfaces of cicada

Psaltoda claripennis wings were demonstrated to mechanically kill pathogenic bacteria *Pseudomonas aeruginosa* American Type Culture Collection (ATCC) 9027 and the drug-resistant *Escherichia coli* K12.^[12,17] The surfaces of the wings of dragon- and damselflies, e.g., *Diplacoides bipunctata* and *Calopteryx haemorrhoidalis*, exhibited broad-spectrum bactericidal activity toward Gram-positive, Gram-negative, and *Bacillus subtilis* spores, where the bacterial cells and spores were determined to be physically

1. Introduction

Candida spp. are commensal inhabitants of the human microflora that can be detected in the digestive and vaginal tracts.^[1] Although *Candida albicans* is the most prevalent cause of candidemia, more than half of all *Candida* infections are now caused by other *Candida* species;^[2–3] particularly multi-drug resistant *Candida auris*.^[2–4] Multi-drug-resistant *Candida*-related

P. H. Le, A. Aburto-Medina, R. J. Crawford, E. P. Ivanova
 School of Science
 STEM College
 RMIT University
 Melbourne, VIC 3000, Australia
 E-mail: elena.ivanova@rmit.edu.au

P. H. Le, D. P. Linklater, A. Aburto-Medina, E. P. Ivanova
 ARC Research Hub for Australian Steel Manufacturing
 Melbourne, VIC 3001, Australia
 D. P. Linklater
 Department of Biomedical Engineering
 The University of Melbourne
 Parkville, VIC 3010, Australia
 S. Nie, N. A. Williamson
 Melbourne Mass Spectrometry and Proteomics Facility
 Bio21 Molecular Science & Biotechnology Institute
 The University of Melbourne
 Melbourne, VIC 3010, Australia
 S. Maclaughlin
 BlueScope Steel Ltd
 Port Kembla, NSW 2505, Australia

 The ORCID identification number(s) for the author(s) of this article can be found under <https://doi.org/10.1002/admi.202300314>

© 2023 The Authors. Advanced Materials Interfaces published by Wiley-VCH GmbH. This is an open access article under the terms of the Creative Commons Attribution License, which permits use, distribution and reproduction in any medium, provided the original work is properly cited.

DOI: 10.1002/admi.202300314

lyzed.^[10,18–20] Currently, an array of diverse biocidal topographies that eliminate attached cells by application of mechanical forces that stretch the cell wall/cell membrane until it ruptures has been developed.^[21–23]

Although eukaryotic yeast cells are structurally different from prokaryotic cells, the “mechano-biocidal” effect of both natural and artificial *nanostructured* surfaces toward *C. albicans* cells has been shown. Nowlin et al. observed that *Saccharomyces cerevisiae* cells were effectively ruptured after 8 h incubation on the surfaces of cicada *Tibicen tibicen* wings.^[24] It was also noted that the biocidal activity of the wing surface patterns of insects such as *Magficicada septendecim* and *Neotibicen tibicen* that possessed nanopillars of lower aspect ratio was comparatively reduced.^[24,25] Indeed, the mechano-bactericidal action of nanostructured topographies has been shown to be dependent on both surface feature size (aspect ratio) and density, as well as the cell morphology and cell wall characteristics of the bacteria.^[13]

Inspired by the mechano-biocidal effect of insect wing topographies, recently, the antifungal activity of nanostructured materials, such as titania (TiO₂) nanotubes^[26] and Ti nanowires,^[27] zinc oxide (ZnO) nanowires,^[28] TiO₂-Cerium oxide (CeO₂) nanofibers,^[29] and graphene^[30] nanocoatings on Ti substrata has also been demonstrated. For example, the graphene nanocoatings exerted a persistent (7-days) inhibitory effect on the biofilm formation on the Ti surface. *Candida* cells attached to the graphene nanocoatings presented as isolated micro-colonies without any hyphal elements. In addition, Yuan and Zhang, who investigated the antifungal mechanism of biomimetic zeolitic imidazolate framework (ZIF) nano-dagger arrays on poly(methyl methacrylate) (PMMA) substratum^[31] observed that the ZIF coating on PMMA exhibited strong fungicidal activity achieved by direct physical contact with the nano-array surfaces. Kollu et al., also demonstrated that pillars of ≈300 nm height exerted sufficient pressure on the *C. albicans* cell membrane to induce cell death.^[25]

By contrast, micro-rough topographies have been shown to increase *Candida* adhesion.^[32–33] A micro-rough topography can increase osseointegration of Ti dental implants by accelerating bone tissue regeneration and increasing the mechanical retention in the bone bed;^[34] however, considering that *Candida* spp. are proficient colonizers of micro-rough Ti surfaces, there are serious implications with regard to infection.^[35–36]

Regardless, the antifungal mechanism of nano- and microstructured topographies, including tubes, wires, pillars, etc., has not been illuminated. *C. albicans* cells were not effectively killed by a microcone array on silicon (Si) substrata as they were observed to rest inbetween the microcones on silicon surfaces (height: 3.5 μm, base width: 630 nm) due to the vast distance (3.7 μm) between the microcones. In addition, *C. albicans* cell wall may be too thick for the tip of the microcone silicon surfaces (tip width: 1–10 nm) to penetrate.^[37] Valdez-Salas et al. demonstrated that Ti nanotubes may disrupt *C. albicans* nanoadhesion bonds at the biointerface and hypothesized that the surface topography and structural orientation play a crucial role in reducing *C. albicans* attachment.^[38] Herein, in light of the mechano-bactericidal action of nanostructured surfaces, we hypothesize that surface features in the order of microns could apply sufficient me-

chanical force to the cell wall of *Candida* cells to promote cell lysis.

In this work, we aimed to fabricate antifungal Ti surfaces with a micro-pillar pattern using maskless chlorine-based inductively coupled plasma reactive ion etching (ICP-RIE). Complementary microscopic techniques, including confocal laser scanning microscopy (CLSM) and scanning electron microscopy (SEM), were used to determine the attachment and viability of two pathogenic *Candida* species over 7 days. Additionally, the *Candida* cells biointerfaces with the micro-pillared surfaces were investigated using focused ion beam SEM (FIB-SEM). Functional proteome analysis of the *Candida* cells interacting with micro-pillared Ti surfaces was conducted to assess the metabolic response of *Candida* cells while interacting with the micro-pillared Ti. Based on the data generated in due course of this study we propose a new mechano-fungicidal mechanism associated with micro-pillared pattern fabricated on Ti surfaces: programmed death of injured *Candida* cells upon interaction with micro-pillared Ti.

2. Results and Discussion

2.1. Surface Characterization of Micro-Pillared Ti

In this study, we developed a micro-pillared Ti surface using a previously optimised ICP-RIE method. The surface topography and architecture of micro-pillar Ti and as-received, non-textured Ti surfaces were characterized using SEM (**Figure 1**) and AFM topographic analysis (Figure S1, Table S2). Analysis of the low- and high-resolution SEM micrographs (Figure 1a,b) revealed the Ti surface to be composed of micron-sized pillars that are clustered to create pyramidal structures. Based on the AFM analysis, primary micropillars were estimated to be ≈760 nm in diameter and 3.5 μm in height (Figure 1b,c). The surfaces of as-received Ti had typical directional depressions caused by the cutting and grinding of the Ti rods with S_a of 418 ± 13.8 nm (Figure S1 and Table S2).

Analysis of the surface wettability determined by measurement of the water contact angle (WCA) of a sessile 10 μL droplet revealed that the surfaces demonstrated a moderate degree of hydrophobicity, exhibiting a WCA of 57° and 65° for as-received Ti and micro-pillared Ti, respectively (Figure 1a; Figure S1). The WCA of micro-pillared Ti surfaces was within the previously observed range.^[22] The elemental analysis of the as-received and micro-pillared Ti surfaces, as performed by X-ray Photoelectron Spectroscopy (XPS), is shown in Figure 1c,f. The XPS spectra revealed two significant doublet peaks characteristic of Ti, including Ti 2p 1/2 and Ti 2p 3/2 (Figure S2) for both surfaces being studied. Furthermore, narrow scans of the O 1s and Ti 2p areas were used to verify the structure of a stable oxide layer (TiO₂). The XPS data confirmed that the chemical composition of the micro-pillared Ti surfaces did not change during the fabrication processes such as grinding, polishing, and plasma etching. The surface characterization including surface roughness and EDS analysis of as-received, micro-pillared Ti and negative control – mirror polished Ti was also provided in Table S2 and S3, and Figure S3, in Supporting Information.

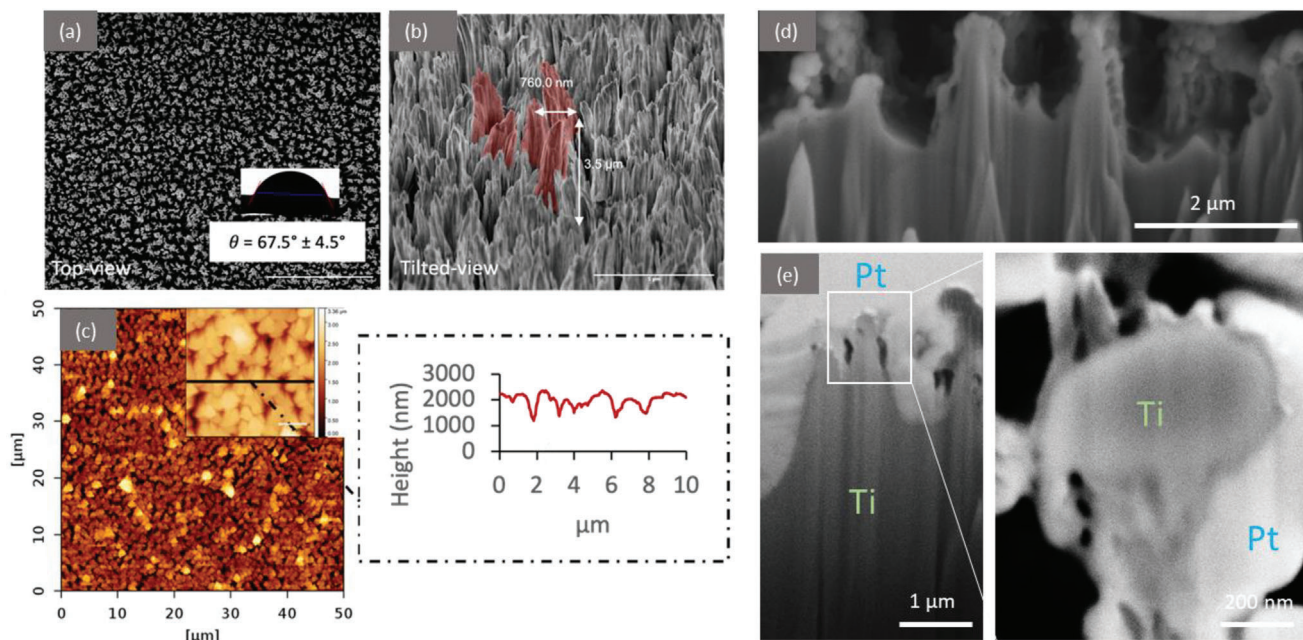


Figure 1. Surface topography, architecture, wettability, and chemical characterization of micro-pillared Ti surfaces. A,B) Representative top-view and tilted (55°) SEM micrographs. Scale bars are 20 μm and 5 μm for top-view and tilted high-resolution micrographs, respectively. The water contact angle (inset to SEM images) showed that micro-pillared Ti surfaces were moderately hydrophobic ($n = 5$). C) Representative 2D AFM micrograph and corresponding AFM line profile. The scale bar of the inset AFM micrograph is 2 μm . D,E) FIB-SEM cross-section of the micro-pillared Ti showing the clustering of the pillars. Platinum and titanium are indicated.

2.2. Attachment of *C. albicans* and *C. auris* and Antifungal Activity of Micro-Pillared Ti

The comprehensive investigation of micro-pillared Ti surfaces' antifungal properties was conducted using direct plate counting, fluorescence and electron microscopy, and proteomics. First, the attachment of *C. albicans* and *C. auris* cells over a 7-day incubation period was assessed. Calcofluor white was used to stain the cell wall of attached *Candida* cells, as it binds specifically to the (1,3)- β and (1,4)- β polysaccharides of cellulose and chitin (Figure S4) and allows the direct visualization and quantification of the cells attached on the sample (Figures 2 and 3). The cell density after Days 1, 3, and 7 of attached *C. albicans* cells on micro-pillar Ti was reduced by $\approx 3\times$ in comparison to the numbers of *C. albicans* cells attached on as-received Ti surfaces (Figure 2b). A 10-fold reduction in attachment was observed ($***p < 0.001$) for *C. auris* cells interacting with micro-pillared Ti substrata (Figure 2b). The quantification of viable *Candida* cells retrieved from the micro-pillared Ti surfaces using the direct plate counting technique revealed a similar trend. Specifically, the number of *C. albicans* cells was 1.3×10^5 and 8.7×10^3 (CFU mL^{-1}) for as-received Ti and micro-pillared Ti, respectively, equating to a 15-fold reduction in attachment on micro-pillared Ti surfaces after 7 days of observation in comparison to the number of cells attached on as-received Ti surfaces (Figure 2a and Figure S5). The number of *C. auris* cells was decreased 5-fold on micro-pillared Ti (8.0×10^3 colony forming units (CFU) mL^{-1}) compared to as-received Ti (4.2×10^4 CFU mL^{-1}) after 7 days incubation (Figure 2a and Figure S5). While the cell density of attached *C. auris* cells on micro-pillared Ti surfaces was observed to increase at day 7 (Figure 2b),

the number of CFU, was decreased, thus indicating that the cells detected on the surfaces were not able to proliferate and form biofilms.^[39] Thus, the micro-pillared Ti surfaces designed and fabricated in this study showed both fungicidal ($\approx 50\%$ of fungicidal efficiency) and fungistatic activity by preventing the proliferation and biofilm formation of remaining cells.

A decreased propensity of *Candida* attachment to hydrothermally etched Ti surfaces and Ti surfaces that featured numerous sharp peaks was also reported previously.^[27,40] It is likely that the reduction in the number of cells attached to the surface is due to a decrease in the surface area available for cell settlement and proliferation.^[41–42] The Ti surfaces fabricated in this study, possessed an array of micropillars that reduced total surface area, whereas the higher attachment density of both *Candida* spp. on the as-received Ti surfaces is most likely due to the presence of numerous shallow pits and valleys (Figure S1), that are comparable with the size of *C. albicans* cells (3–4 μm) and support cell attachment and proliferation.^[40,43]

Further investigation of the *C. albicans* and *C. auris* cells attachment and their physiological status was conducted using CLSM (Figure 3a). Fluorescent labeling with thiazole orange (staining yeast nucleus, in green color) and Live-or-Dye (staining free amines of the intracellular proteins when the cell is non-viable, in red color) was used to discriminate between viable and non-viable cells, respectively.^[40] The proportion of viable *C. albicans* and *C. auris* cells attached to the as-received Ti substrata remained at $\approx 90\%$ or greater over the 7-day incubation period (Figure 3b,d – top panel). In contrast, the proportion of viable *C. albicans* cells was found to be 70% on Day 1, 44% on Day 3, and then $\approx 51\%$ and 58% on Day 5 and Day 7, respectively (Figure 3b – bottom

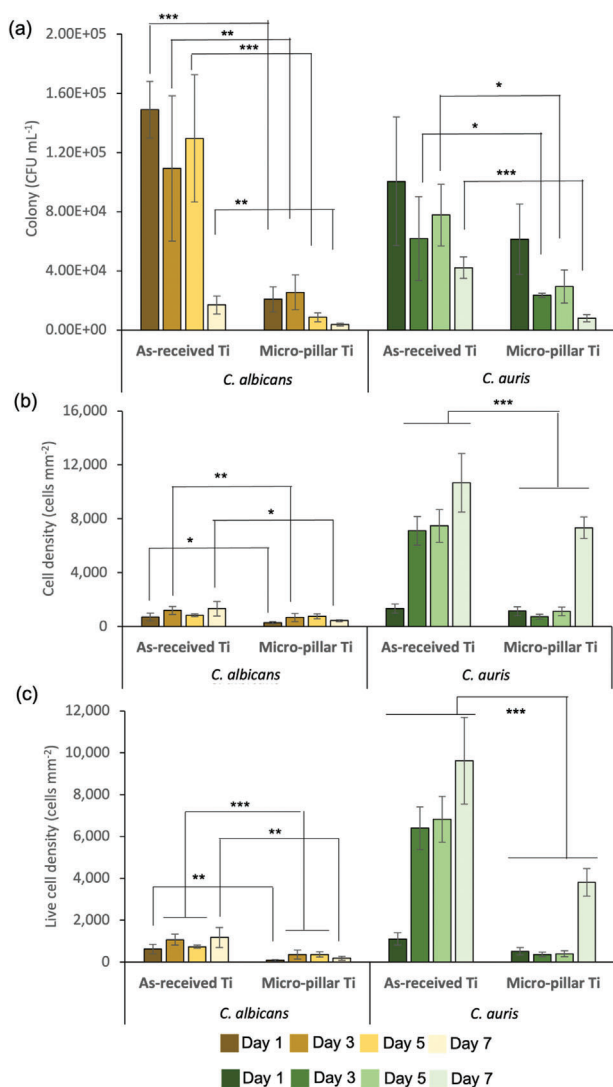


Figure 2. Attachment of *C. albicans* and *C. auris* cells. A) Quantification of *C. albicans* and *C. auris* CFU mL⁻¹ on the as-received Ti and micro-pillar Ti surfaces over a 7-day incubation. B) Quantification of total number of attached *C. albicans* and *C. auris* cells on the as-received Ti and micro-pillar Ti surfaces by fluorescence microscopy. The data were derived from the analysis of the CLSM micrographs ($n = 15$). C) The number of viable attached cells of *C. albicans* and *C. auris* on the as-received Ti and micro-pillar Ti surfaces over a 7-day incubation. The number of live cell densities was calculated using the CLSM micrographs ($n = 15$). Three independent technical repeats were carried out ($n = 5$). Statistical significance is indicated by *** $p < 0.001$, ** $p < 0.01$, * $p < 0.05$.

panel). Furthermore, the number of non-viable *C. auris* cells on micro-pillar Ti was $\approx 55\%$, 50% , 64% , and 48% on Day 1, Day 3, Day 5, and Day 7, respectively (Figure 3d – bottom panel). Thus, these data indicate that the micro-pillar Ti can directly and persistently kill $\approx 50\%$ of attached cells of both *Candida* strains, and effectively deter microbial proliferation and biofilm formation.

Since *Candida* cells attached to abiotic or biotic surfaces create micro-colonies and secrete capsular extracellular polymeric substances (EPS) in order to facilitate their attachment and biofilm formation,^[44] the production of EPS was visualized by fluores-

cent staining with Concanavalin A (Figure 4). Analysis of CLSM micrographs showed that both *C. albicans* and *C. auris* cells secreted elevated levels of EPS after 3 days of incubation on the as-received Ti surfaces (Figure 3a,b, orange arrow in as-received Ti panel). By contrast, the production of EPS by *Candida* cells attached to the micro-pillar Ti surfaces was negligible, even on Day 7 (Figure 4a,b, in micro-pillar Ti panel).

A laser-structured micro-pillar Ti substratum with average surface roughness in the order of $6\text{--}8\ \mu\text{m}$ was recently demonstrated to reduce the adhesion and proliferation of *C. albicans*, effectively preventing biofilm formation.^[45] Analysis of cell attachment and morphology revealed an increased extent of disorganization and spacing between fungal cells and a reduction in cell density. Importantly, the authors noted the absence of hyphae and pseudohyphae. It was hypothesized that the inhibitory effect of the laser-structured Ti surfaces could partly be attributed to the presence of titanium nitride and/or oxides on the surface.

As the surface chemistry and wettability of the Ti substrata remained unchanged following the surface modification process (Figure S2b and Table S3), our data suggests that the micropillar topology played a significant role in facilitating the antifungal activity of the micro-pillar Ti substrata against both *Candida* species, preventing their attachment, proliferation, and biofilm formation.

2.3. Cell Morphology of *C. albicans* and *C. auris* on Micro-Pillared Ti Surfaces

SEM analysis of *Candida* cell morphology, when attached to the micro-pillar Ti surfaces, revealed the deformed shape of both cell strains (Figure 4c,d, highlighted in red in micro-pillar Ti panel) in comparison to the *Candida* cells attached on as-received Ti (Figure 4c,d, yellow arrows in as-received panel). Here, both *C. albicans* and *C. auris* cells appeared lysed upon attachment to the micro-pillar Ti surfaces. In agreement with CLSM imaging, *Candida* cells on micro-pillar Ti surfaces did not appear to have produced any EPS, whereas *C. auris* cells on as-received Ti surfaces are enclosed in an EPS matrix from Day 3. Both *C. albicans* and *C. auris* were only observed as spherical yeast cells on micro-pillar Ti surfaces. By contrast, *Candida* cells on as-received Ti surfaces exhibited a budding yeast phenotype (yellow arrows; SEM images; Figure 4c,d and Figure S6). Both *C. albicans* and *C. auris* form ovoid-like cells that proliferate by budding.^[46] The budding yeast phenotype critically indicates the production of daughter cells and the proliferation of the yeast population on the substratum.^[46] True hyphal forms exhibit a homogeneously elongated shape and lack of constrictions at a solid septum.^[46]

2.4. Functional Proteomic Analysis of Differentially Expressed Proteins in *Candida* on Micropillar Ti Surfaces

Given that the micro-pillar Ti surfaces display both fungicidal and fungistatic activity, a functional proteome analysis was used to identify the involvement of proteins in a range of complex pathways pertaining to cell attachment, metabolism, motility, proliferation, and cell stress (Figure 5).^[47] As *C. albicans* and *C. auris* cells could excrete EPS on the as-received Ti, but not on the

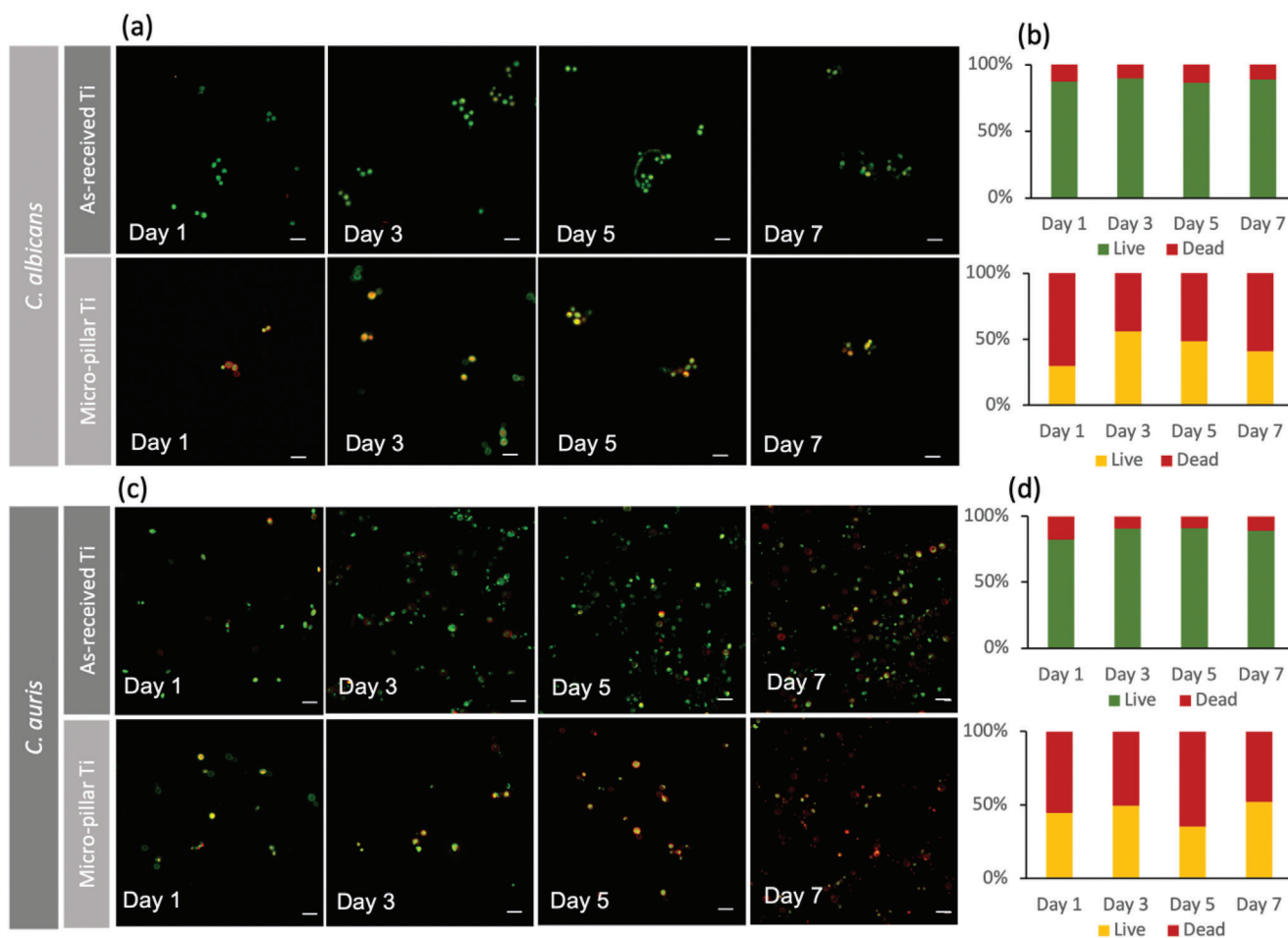


Figure 3. Physiological status of *C. albicans* and *C. auris* cells attached to as-received Ti and micro-pillar Ti surfaces over the 7-day incubation. a,c) Representative CLSM micrographs showing the proportion of live/dead a) *C. albicans* and c) *C. auris* cells attached to as-received Ti and micro-pillar Ti surfaces at four discrete sampling points. CLSM images are merged channels, where live cells are green, dead cells are red, and compromised cells are orange. b,d) The proportion of live/dead attached b) *C. albicans* and d) *C. auris* on as-received Ti and micro-pillared Ti surfaces. *C. albicans* and *C. auris* cells attached to the as-received Ti displayed high levels of viability, as seen by the dominance of the green color. In contrast, the cells attached to the micro-pillared Ti substratum showed a consistent proportion of dead cells (red color) and the cells with a compromised outer layer/and membrane (orange color) that were damaged as a result of interacting with the micro-pillared Ti surface. The quantification of live and dead cells was conducted using the CLSM micrographs ($n = 15$).

micro-pillar Ti surface after 3 days, the cells were collected for proteomics analysis at this time point.

Proteins involved in carbohydrate and lipid metabolism, entry to cells' stationary phase, and stress response to an external stressor were considerably upregulated for *Candida* cells of both strains on micro-pillar Ti surfaces. At the same time, the expression of proteins involved in the development of the cytoskeleton including actin filaments and microtubules, and biosynthesis processes were inhibited (Figure 5c).

Specifically, functional proteomic analysis of *C. albicans* following interaction with the micro-pillar Ti revealed significant up-regulation of ADF-H domain-containing protein, of the ADF/cofilin protein family that is involved in the actin filament debranching process.^[48–49] The formation of the branched actin networks is essential for cell polarity. Cell polarity in yeasts is in turn essential for cell mobility, and proliferation.^[46] Proteins that depolymerize actin filaments are up-regulated during periods of

cytokinesis, cell motility, and extreme stress.^[49] As our study has shown that *Candida* cells on micro-pillared Ti surfaces do not form the yeast budding phenotype and, therefore, are not actively undergoing cytokinesis, it is likely that actin filament debranching was incurred because of cell stress. In fact, our prior research revealed that nanoscale surface architectures with a larger ratio of peaks to valleys were not only resistant to *C. albicans* attachment but also acted as an exogenous stress factor, triggering an altered actin cytoskeleton network in attached yeast cells.^[43] Similarly, microtubule-associated proteins MHP1P/MAP-homologous protein 1 were also up-regulated. Over-expression of these proteins is commonly involved with cell-cycle arrest in times of stress.^[50–52] There was also elevated production of a few other proteins involved in halting the cell cycle, such as protein kinases that depress stress-induced genes^[53] as well as amino-acid permease GAP6, which plays a role in activation of such protein kinases.^[54] Evidence of cell cycle arrest and cell stress was further associated

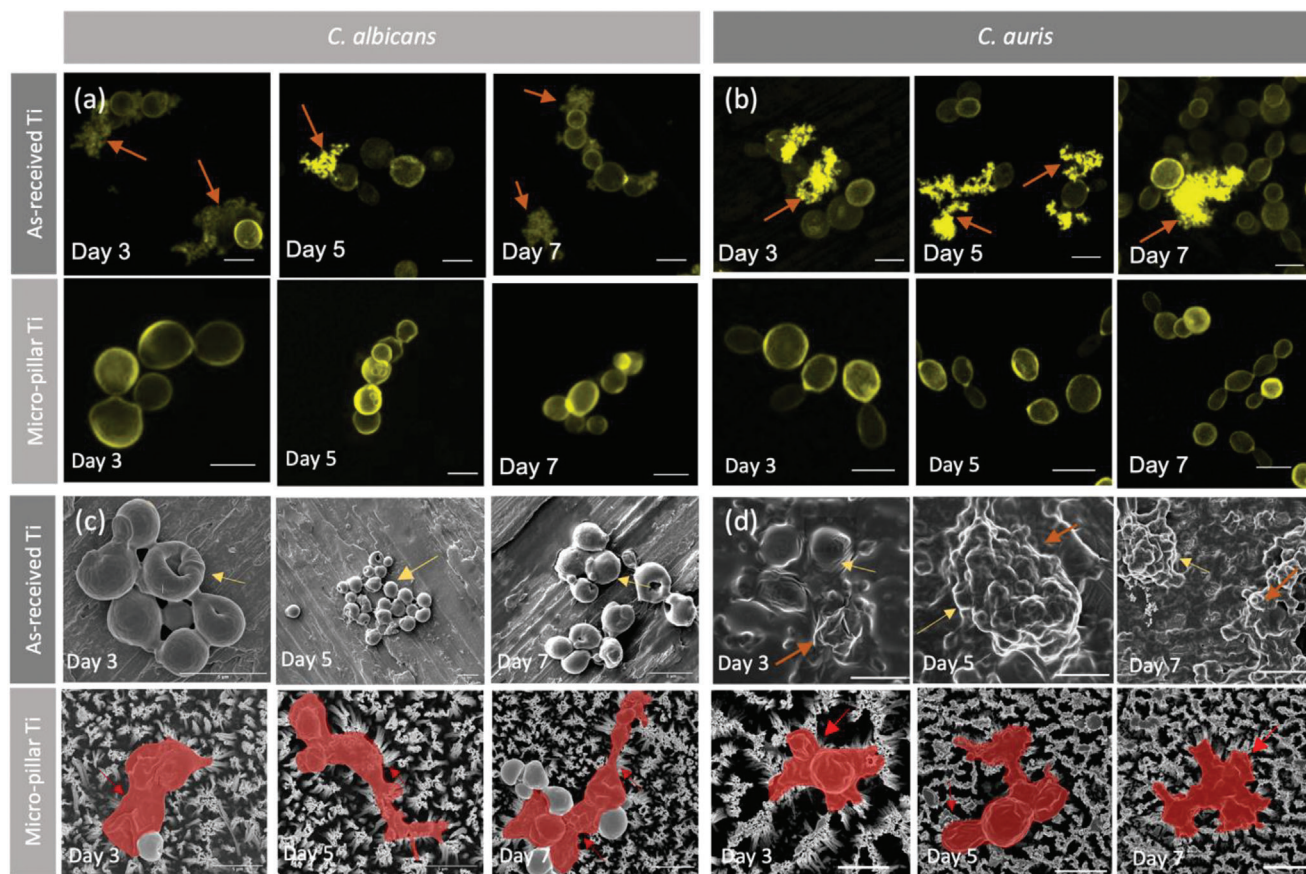


Figure 4. Cell morphology and EPS production of attached *C. albicans* and *C. auris* cells on the as-received Ti and micro-pillared Ti surfaces over 7 days. a,b) Fluorescent micrographs of capsular and extracellular EPS produced by *C. albicans* and *C. auris* on micro-pillar Ti and as-received Ti surfaces over 7 days incubation. *Candida* cells were stained with Concanavalin A, which specifically binds to α -mannopyranosyl and α -glucopyranosyl glycoproteins (components of biofilm). EPS production is indicated by the orange arrows. Both types of yeast cells started to secrete EPS after a 3-day incubation period on the as-received Ti surfaces, but not on the micro-pillar Ti surfaces. Scale bars are 5 μ m. c,d) Representative SEM micrographs of the morphology of *C. albicans* and *C. auris* cells attached on the as-received Ti and micro-pillar Ti surfaces. The *C. albicans* and *C. auris* cells that attached to the as-received Ti surfaces presented an elongated shape with surface buds, indicating that they were able to produce daughter cells (yellow arrow). The *C. albicans* and *C. auris* cells attached onto the micro-pillar Ti surface appeared deformed after attachment on the micropillars (false-colored red and red arrow). Scale bars are 5 μ m.

with the down-regulation of certain proteins, required for the development of the *Candida* filamentous/hyphae phenotype that is required to form biofilm^[55] (Figure 5c).

Elevated levels of proteins involved in vacuolar transport, amino acid transmembrane transport, and intracellular protein transport, and the transmembrane transport proteins that are required for the transfer of ions, micro- and macromolecules across the cell membrane were also noted (protein identification can be found in Table S3).^[56] Two other up-regulated proteins, which are part of the endoplasmic reticulum through Golgi vesicle-mediated transport process,^[57] may be involved in the synthesis of carbohydrate molecules, in the carbohydrate metabolic process and in cellular lipid metabolism (Table S3). These proteins may be also associated with the general amino acid control system, which responds to deprivation in yeast cells by blocking translation initiation and accumulating the activator protein Gcn4.^[58] Gcn4 expression can be triggered by a variety of additional stressors that limit translation, one of which is oxidative stress.^[59] For example, it was found that TiO₂ nanopillars induced bacte-

rial cell envelope deformation of both Gram-positive and Gram-negative bacteria and caused oxidative stress.^[60] It was also reported that attachment of bacterial cells on sharp structures^[61] or silver-coated carbon nanotubes^[62] was associated with a stress response, manifested as an impairment in processes like microbial proliferation and biofilm formation.

2.5. Apoptosis – Programmed Cell Death of *Candida* Cells Induced by Micro-Pillar Ti

Apoptosis, also known as programmed cell death, has been researched intensively for yeasts in recent years.^[64–66] It is a manner of cellular suicide whose process is intimately associated with the eradication of damaged cells.^[67] Yeast apoptosis may be initiated by external stimuli such as physical stress.^[66] Herein, we postulate that *Candida* cells that are not immediately killed by the stretching action of the Ti micro-pillared array may undergo programmed cell death because of sub-lethal injury incurred dur-

ing attachment to the microtextured surface because of their inability to be revived in a stress-free environment post incubation on micro-pillar Ti surfaces. We recently demonstrated that bacteria exposed to nanopillar silicon surfaces that incurred a mechanical injury not sufficient to kill the bacteria instead underwent programmed apoptosis-like death (ALD). In addition, when the mechanical stress was removed, the self-accumulated reactive oxygen species (ROS) incurred post-stress ALD in damaged cells.^[68]

It is well known that the expression of metacaspases is necessary as one of the fundamental processes associated with apoptosis in yeast cells.^[69] It is likely that activated caspase 1, activates “cell death executor” gasdermin D, which is initiated pore formation in the cell membrane leading to cytosol leakage and cell death. Our functional proteome analysis revealed that the metacaspases-1 protein (Yca1p) was expressed by both *C. albicans* and *C. auris* on micro-pillar Ti (protein ID: Q5ANA8 and A0A0L0NNH3 for *C. albicans* and *C. auris*, respectively). The expression of this protein is a strong indicator of the activation of the apoptosis pathway in *Candida* cells adhering to micro-pillar Ti.^[66]

Certain key cellular pathways such as DNA replication, mitochondrial activity, RNA, and protein stability, appear to be negatively impacted by the expression of metacaspases.^[69] In fact, *Candida* cells attached to micropillar Ti over-expressed proteins associated with these biological processes (Table S3). In terms of DNA replication, *C. albicans* up-regulated expression of DNA replication licensing factor MCM2 and elongator subunit proteins, which are critical for the replication process. The turnover rate of certain mRNAs influences the amounts of protein expression, and perturbing this process may have profound effects on gene expression.^[69] mRNA turnover in yeast involves many decay mechanisms, including 3′/5′ exonucleolytic digestion.^[70] These effects result in the emergence of apoptotic phenotype and the acceleration of chronological deterioration.^[71] Herein, exosome complex exonuclease RRP41 was shown to be up-regulated in *C. albicans* cells; this protein is accountable for the 3′-5′ exonucleolytic nonsense-mediated decay pathway. In addition to protein stability, one of the biological mechanisms controlling the cell death pathway is the ubiquitin (Ub)-mediated covalent modification (ubiquitination).^[69] Proteomic analysis revealed that several proteins involved in the proteasome-mediated ubiquitin-dependent protein catabolic process were up-regulated in *Candida* exposed to micropillar Ti surfaces. These proteins include the ubiquitin-specific protease expressed by *C. albicans*, as well as the UBX domain-containing protein and Pru domain-containing protein expressed by *C. auris*. It was also found that *C. auris* cells exhibited a high level of cytochrome b pre-mRNA-processing protein 6, which is responsible for protein stabilization.

It is widely known that mitochondria play a major role in regulating the cell death response.^[69,72] The activation of metacaspases in reaction to hyperosmotic stress requires the release of cytochrome c from mitochondria.^[72] It was observed that *C. auris* expressed the UCR hinge domain, which is involved in the biological process of ubiquinol cytochrome c reductase that is triggered by mitochondria. Significantly, both *C. albicans* and *C. auris* cells produced a significant number of proteins associated with the above-mentioned mitochondrial activities (Table S3).

The clustered protein network shown in Figure 5d demonstrates that there were significant correlations between the proteins produced by *C. albicans* in response to cell disruption and leading to apoptosis. Specifically, the disruption of the cell wall generated by micro-pillared Ti led to the production of proteins involved in cellular lipid metabolic, carbohydrate derivative metabolic, and biotin biosynthetic activities in order to promote the rebuilding of the cell membrane. Those proteins involved in intracellular protein transport and stress response indicate that cells were subjected to physical stress induced by micropillars. The expression of several proteins, including metacaspases and those involved in the mRNA process, chromatin remodeling, and nucleosome assembly, provides compelling evidence that *C. albicans* cells were undergoing apoptosis (Figure 6). Consequently, it is hypothesized that the micro-pillar Ti not only produced the collapse of the cell wall but also induced programmed cell death – apoptosis.

Additionally, chromatin condensation is another characteristic indication of yeast apoptosis.^[69] YL1-C and NGG1, a subunit of a chromatin-remodeling complex, were both considerably up-regulated in *C. albicans* cells attached to Ti micro-pillared surface. Chromatin remodeling is the reorganization of chromatin from a condensed to a transcriptionally appropriate form, enabling transcription factors to regulate gene expression.^[73] It indicates that the chromatin structure of *C. albicans* cells appeared to be in a dense condition, forcing the expression of these proteins in order to rearrange their chromatin network.

2.6. Investigation of the *Candida*-Micropillar Ti Biointerface

The biointerface of Ti micropillars and *Candida* cells was further investigated using cross-sectional FIB milling of the cell-surface interface. FIB SEM was used to gain insight into the interactions between the attached *Candida* cells and the Ti micropillars that would result in the cell deformation as observed in the SEM images in Figures 4c,d and 6. Sequential milling of the cell-surface interface revealed that when *C. albicans* and *C. auris* cells encountered the Ti surface micropillars, the homogenous line of their cell walls was disrupted (Figure 7). It is clearly observed that the cell walls of *C. albicans* and *C. auris* cells were indented at the point of attachment to the micropillar surface causing an irregular morphology of the cell wall as indicated by the yellow dashed line (Figure 6). In the case of *C. auris* cell, which was at the advanced stage of the interaction with the micropillars, the micropillars appeared to penetrate the cell wall, as a loss of cell wall and membrane integrity was observed. In addition, the irregular top surface of the cells that had attached to the micro-pillar Ti suggested a loss of turgor pressure, which is related to cell rupture. In contrast, the cell wall of cells attached onto the as-received Ti appeared in a healthy shape without any damage, at the surface attachment points (Figure S5, yellow dashed line). A similar observation of stretched and distorted *C. albicans* cell membrane during interactions with nanostructured surfaces of *T. tibicen* wing was observed by Nowlin et al, proven by FIB-SEM micrographs, where the *C. albicans* cell membrane was significantly stretched and distorted across the nanoscale protrusions on the wing surface.^[24] It has been shown that nanostructured surfaces with features that have a larger

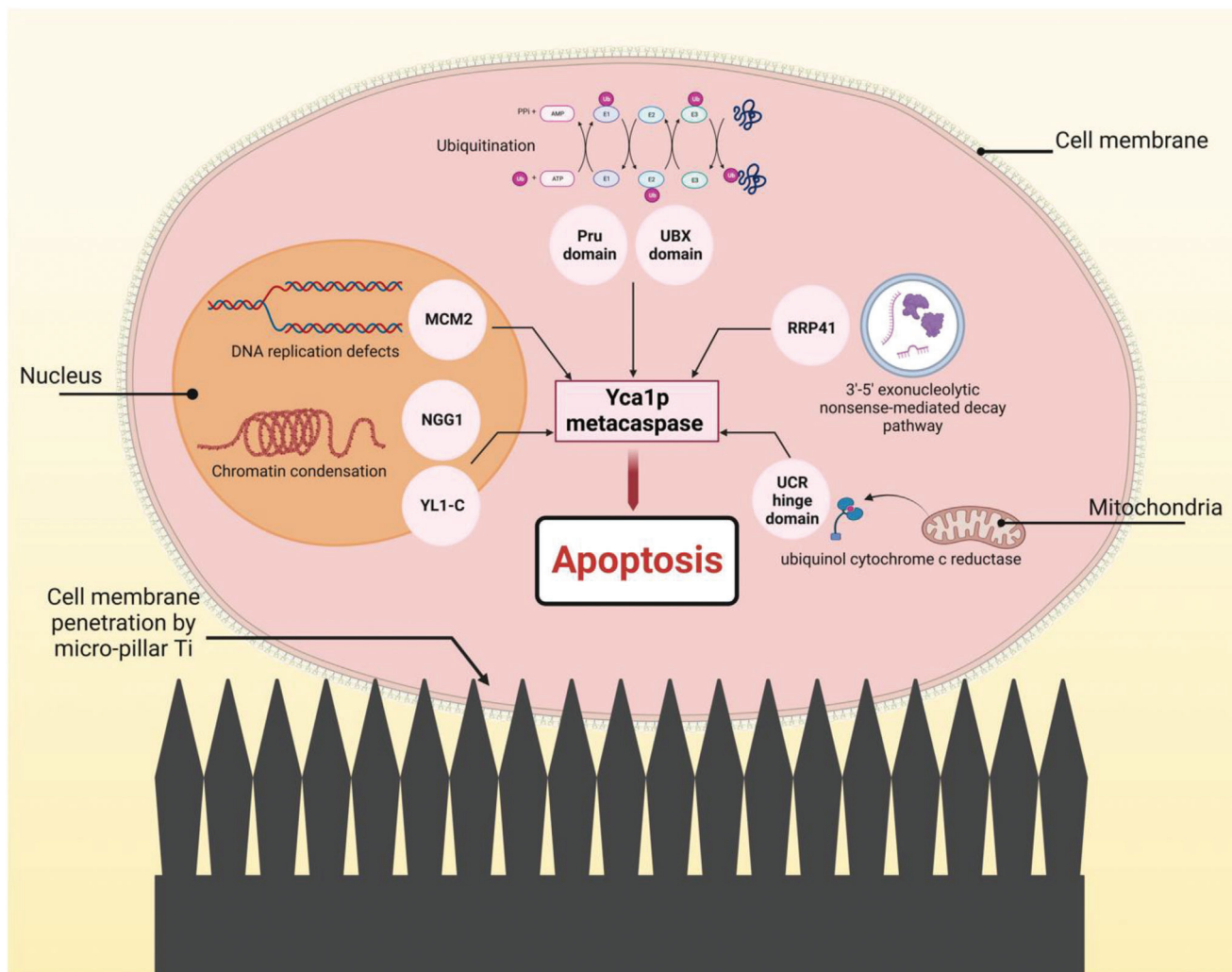


Figure 6. Cellular targets of metacaspases-dependent of *Candida* apoptosis interacting with micro-pillar Ti surfaces. Activation of YCA1 appears to be associated with impairments in various critical cellular processes such as DNA replication (indicated by MCM2 protein), mitochondrial function (indicated by UCR hinge domain protein), RNA stability (indicated by RRP41 protein), protein stability (indicated by Pru and UBX domains), and chromatin condensation (indicated by YL1-C and NGG1 proteins), which are all associated with yeast apoptosis. The expression of these proteins provides strong evidence that *Candida* cells underwent apoptosis. Created with BioRender.com.

aspect ratio than those with a lower aspect ratio may induce increased cell rupturing.^[14,24] Herein, the Ti micropillars are considerably higher aspect ratio, more rigid, and broader in diameter (3.5 μm in height and clustered tips of ≈760 nm in width) compared to those nanostructured features on insect wings. Although physical penetration of the micropillars into the cell membrane is unlikely due to the large tip diameter, it is assumed that mechanical deformation of the *Candida* cell wall as it adsorbs to the micropillar surface leads to a significant stress response, and ultimately programmed cell death.

3. Conclusion

Herein, the micro-pillar Ti surfaces exhibited remarkable antifungal properties against two pathogenic yeasts, *C. albicans*, and multidrug-resistant *C. auris*. Micro-pillar Ti surfaces demonstrated both fungistatic and fungicidal behavior, being able to sus-

tainably eliminate ~50% of *Candida* cells upon attachment and, at the same time, prevent yeast cells from forming a biofilm over a 7-day incubation. Functional proteome analysis revealed that the yeast cells were under external stress while interacting with micro-pillar Ti surfaces and expressed elevated levels of protein involved in cell cycle arrest and apoptosis. We propose a new mechano-fungicidal mechanism associated with micro-pillared surfaces: programmed death of injured apoptotic cells via pyroptosis resulting in the pore formation in the cell membrane, leading to cytosol leakage and cell death. The apoptosis is associated with down-regulated proteins that are involved in development of filamentous/hyphae shape biofilm phenotypes of yeast cells, thus confirming that the yeast cells were unable to form a biofilm. This is the first example of a micro-pillared surface with biofilm-resistant properties that is also capable of mechanical rupturing and/or injuring yeast cells and persistently deterring their proliferation.

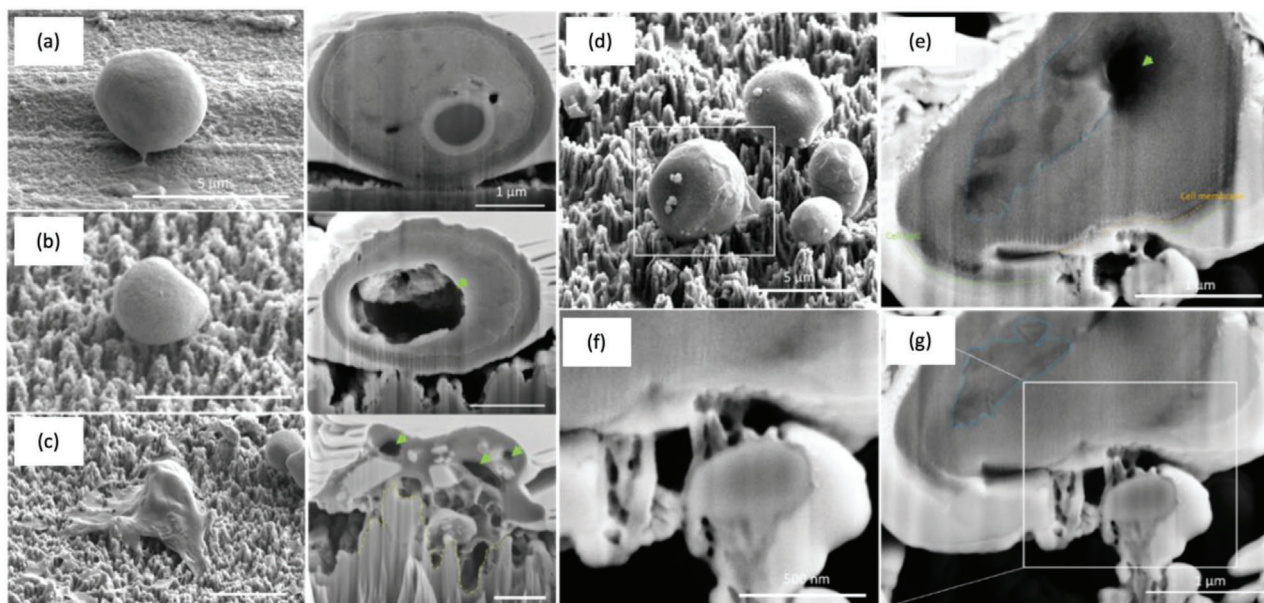


Figure 7. Representative SEM micrographs of FIB milling of the cell-micropillar interface of *Candida* cells attached to micro-pillar Ti surfaces. a) The cell morphology and ultrastructure on control, as-received Ti surfaces. b) A *Candida* cell on a micro-pillar Ti surface with a large cytoplasmic vacuole (green arrow) and ultrastructural degradation. Micro-pillars are in direct contact with the cell wall. c) Advanced state of cell death on micro-pillar Ti surfaces. Cross-sectional image shows collapse of cell structural integrity, and many internal vacuoles (green arrows). d–g) High-resolution (HR) FIB-SEM micrographs demonstrating the breakdown of the cell wall (green dashed line) and cytoplasmic membrane (yellow line) of *Candida* in contact with the micropillars (white dashed line). The micro-pillars are observed inserted into the cell cytoplasm. The nucleus appears condensed (blue outline), evidence of chromatin condensation and a hallmark of apoptosis.

4. Experimental Section

Surface Preparation and Fabrication: Commercially pure (CP) ASTM Grade 2 titanium (Ti) rods, 1 cm diameter (Goodfellow, UK) were cut into discs $\approx 1 - 1.5$ mm thickness using a Secotom-50 (Struers, U.S.A.). These referred to as as-received Ti discs were washed with MilliQ water (Resistivity: 18.2 M cm, 25 °C) and then sterilized by sonicating for 15 min in 100% and 70% ethanol (EtOH) (Chem-supply, Australia). After drying at room temperature overnight, the as-received discs were placed in a desiccator to prevent any adsorption of moisture. No further surface changes were made to this group, which was used as a control in all experiments.

To produce micro-structured surfaces, the as-received Ti surfaces were polished to mirror finish (polished Ti). The initial grinding and polishing process was conducted as shown in Table S1. Prior to processing, samples were sonicated successively in acetone, isopropanol, and deionized water for 10 min each time. Some polished Ti surfaces were retained for control experiments, while the remainder was subjected to reactive ion etching for the fabrication of micro-pillar Ti surfaces.

Modification of the polished Ti substrata to impart a surface microstructure was achieved using a chlorine-based, maskless plasma etching technique using Oxford Instruments (Plasmalab System 100) as previously described by Linklater et al.^[22] Briefly, the polished Ti discs were placed on a quartz carrier wafer and subjected to reactive ion etching (RIE; Plasma Lab System 100, Oxford Instruments, U.K.), using Cl_2 gas maintained at a flow rate of 30 standard cubic centimeters per minute (sccm), 1000 W ICP, and 100 W RF power, and 7 mTorr pressure for 40 min. The micro-pillar Ti discs were stored in a desiccator to prevent any moisture from being present on the surface of the discs.

Surface Characterization: A FEI Verios 460L XHR scanning electron microscope (SEM) mounted with Oxford X-Max20 Energy Dispersive X-Ray Detector (EDX) was used to obtain typical surface micrographs and the survey elemental compositions for all the sample surfaces at 3 kV under 1000 \times magnification in high vacuum condition. Surfaces were stored in a

vacuum chamber overnight before use to remove any debris attached to surfaces.

Atomic Force Microscopy: The surface topography of the substrata was characterized using a NanoWizard 4 tip scanning atomic force microscope (JPK BioAFM Business, Bruker NanoGmbH, Germany). The AFM head was placed on an upright optical microscope (IX81, Olympus, Japan), and the tests were conducted in an acoustic hood and on an active vibration isolation table (Accurion, Germany). The scans were carried out in an air-conditioned environment at a temperature of ≈ 25 °C using an n-type antimony-doped silicon probe (SICON, AppNano, USA) in the Quantitative Imaging (Qi) mode. The spring constant of the cantilever was $0.10.6 \text{ N m}^{-1}$. Triplicate scans of each surface were collected across a $50 \times 50 \mu\text{m}^2$ scan area, and a set of roughness characteristics, including average roughness (S_a), root mean square roughness (S_q), and maximum height (S_{max}), were then calculated.^[74,75] Gwyddion (ver. 2.53) was used to analyze the AFM images.^[76]

Surface Wettability: After air drying overnight, the water contact angles of the surfaces being studied were determined. The static water contact angle was determined for each sample using the sessile drop technique. Contact angles were determined using a Phoenix-MT(T) instrument (SEO Co., Korea) coupled with SurfaceWare 9 software. Within two seconds of the $10 \mu\text{L}$ droplet touching the surface, the static water contact angles were measured. The results were an average of five independent measurements taken on each sample.

X-Ray Photoelectron Spectrometer: The elemental analysis of the sample surfaces was performed using a Thermo Scientific K-alpha X-ray photoelectron spectrometer (XPS) (Thermo Fischer Scientific, USA). The K-alpha EPS equipment was equipped with a 150 W monochromatic X-ray source (Al K, $h\nu = 1486.6 \text{ eV}$). The photoelectrons released at 90 degrees to the surface from a $400 \times 400 \mu\text{m}^2$ area were analyzed at 200 eV for survey spectra and subsequently at 50 eV for region spectra. Survey spectra were collected at a resolution of 1.0 eV per step, whereas region spectra were collected with a precision of 0.1 eV per step. The relative atomic concentrations of elements as determined by XPS were quantified using

the peak area in the designated high-resolution zone and the instrument-specific sensitivity settings. Each of the titanium 2p, carbon 1s, and oxygen 1s peaks were scanned with high resolution.

Yeast Strains, Culture Conditions, and Sample Preparation: *Candida albicans* ATCC 10231 samples were purchased from the American Type Culture Collection (ATCC, Manassas, Virginia, USA), and *Candida auris* DSM 21092 samples were purchased from the DSMZ – German Collection of Microorganisms and Cell Cultures GmbH (Leibniz Institute, Germany). The yeast stocks were prepared in 20% glycerol nutrient broth (Oxoid, USA.) and stored at $-80\text{ }^{\circ}\text{C}$. To ensure their purity, two separate samples were taken from the glycerol stock for subsequent growth on potato dextrose agar (PDA) plates (Neogen Culture Media, Australia), at $35\text{ }^{\circ}\text{C}$ for 24 h. One colony was sampled from these plates and transferred to sterile potato dextrose (PDB) medium (Neogen, Australia), pH 7.2 – 7.4, then the cell density of the working suspension was adjusted to $\text{OD}_{600} = 0.1$ ($\approx 10^6$ cells mL^{-1}) using a UV-VIS Halo DB-20 spectrophotometer (Dynamica, UK).

Inoculation of the micro-pillar Ti, as-received Ti, and polished Ti discs with yeast cells was carried out as follows: the sterile surfaces were placed within a Costar 24-well plate (Corning, USA) and immersed in 3 mL yeast cell suspension. The samples were incubated at $35\text{ }^{\circ}\text{C}$ for 1, 3, 5, and 7 days in duplicate, in a humid environment to minimize any evaporation of the fungal suspension. After incubation and prior to cell attachment analysis, the samples were washed gently three times with 3 mL of MilliQ water to remove any non-attached cells. Three independent technical measurements were carried out. The data on polished titanium surfaces (negative control) are reported in Tables S1 and S2 and Figures S3, S7 and S8 (Supporting Information).

4.0.0.1. *C. albicans* and *C. auris* Cell Attachment: To observe the cell morphology and extent of attachment using scanning electron microscopy (SEM), samples were incubated as described above and then fixed with 2.5% glutaraldehyde for 1 h at room temperature, followed by dehydration with graded ethanol (EtOH) series of 30, 50, 70, 90, and 100% for 15 min each. The samples were subsequently sputter coated with Iridium (Ir) at a thickness of 7 nm using an EM ACE600 sputter coater (Leica, Germany). Imaging using the FEI Verios 460L XHR scanning electron microscope was performed at 3 kV. The beam current was kept at 50pA, and a thermoluminescent dosimeter was used as the detector for this SEM investigation.

Confocal Laser Scanning Microscopy: A Zeiss LSM 880 Airyscan up-right confocal laser scanning microscopy (CLSM) system (Carl Zeiss Microscopy, Germany) equipped with a 63 water-immersion objective (ZEISS 60/1.0 vis-IR) was used to visualize attached cells on surfaces. The examined surfaces were carefully washed three times (3 mL each) with MilliQ water to remove non-attached cells and then put in a 3.5 mm glass-bottomed Petri dish filled with 3 mL MilliQ water. Yeast Live-or-Dye Fixable Live/Dead staining kit (Biotium, USA) was used to differentiate between the live and dead cells. The live cells will remain green-colored, the dead cells will be stained red, and the cells possessing a compromised membrane will appear an orange color due to the overlap of the green and red fluorescence signals. Calcofluor white (Biotium, USA.), and Concanavalin A (ConA) CF Dye Conjugates (Biotium, USA) were used to stain the cell wall and extracellular polymeric substances (EPS), respectively. The number of attached *C. albicans* cells to surfaces were quantified using fifteen different fields of view of $135 \times 135\text{ }\mu\text{m}^2$ for each sample. To detect and count attached cells from CLSM micrographs, a cell counter plugin in ImageJ 1.52a was utilized. The total number of attached cells was estimated using both living and dead cell counts. The average of at least three independent technical replicates with duplicates of each type of surface was used to generate the data.

Focus Ion Beam-SEM: FEI Scios DualBeam focus ion beam (FIB) SEM was used to visualize the interaction between the cell wall and surface topography. After being incubated in *C. albicans* and *C. auris* suspensions for 3 days, surfaces were taken out and washed three times with phosphate-buffered saline (PBS). For primary fixation, samples then were fixed with 4% paraformaldehyde and 2.5% glutaraldehyde for at least an hour at room temperature. Samples were rinsed three times with cacodylate buffer. In terms of post-fixation, samples were subsequently fixed with 1.5% potassium ferrocyanide and 2% osmium tetroxide (OsO_4) for an hour before being incubated with freshly made 1% thicarbonylhydrazide in

ddH_2O for 20 min at room temperature. After that, samples were fixed with 2% OsO_4 in MilliQ water for 30 min at room temperature. Samples were rinsed three times with MilliQ water after these steps. The samples were then dehydrated in a series of ice-cold ethanol (EtOH) solutions at 20%, 50%, 70%, 90% to 100% for 5 min for each step. Before the FIB-SEM experiment, samples were air-dried and coated with 10 nm thickness Ir.

Antifungal Activity: The antifungal activity of micro-pillar Ti against both *C. albicans* ATCC 10231 and *C. auris* DSM 21092 was investigated using the spread-plate counting method. This technique was used to confirm the cell viability of attached cells on studied surfaces. All materials and glassware were sterilized before use, and the whole process of plate spreading was conducted inside a safety cabinet to prevent any contamination. The OD of the *Candida* working suspension was adjusted to 0.1 ($\approx 10^6$ cells mL^{-1}) using a UV-VIS Halo DB-20 spectrophotometer (Dynamica, UK). The micro-pillar Ti, as-received Ti, and polished Ti discs were inoculated with yeast cells as follows: the sterile surfaces were put into a Costar 24-well plate (Corning, U.S.A.) and submerged in 3 mL yeast cell solution. micro-pillar Ti, as-received Ti, and polished Ti (positive control) were incubated in *C. albicans* and *C. auris* suspension for 1-, 3-, 5-, and 7-day incubation periods in duplicate. Incubated surfaces then were washed three times with MilliQ water (1.5 mL) to remove any loosely attached cells. Surfaces were transferred to a 15 mL falcon tube and immersed in MilliQ water (1 mL). To remove any attached cell from the studied surface, the falcon tube was vortexed for 2 min at max speed.^[77] Vortexed surfaces were checked using SEM to ensure the absence of any remaining cells on the surfaces or aggregates (Figure S9). After this, 100 μL of diluted suspension (Dilution factor: 10^2) was used to spread on a fresh agar plate using a plate spreader. The plates were then incubated at $37\text{ }^{\circ}\text{C}$ for 48 h before counting the resulting colonies. Experiments were conducted in triplicate, and at least five agar plates for each type of surface were used for the statistical analysis.

The plates were photographed digitally, and the colony forming units per milliliter were manually computed to provide the mean and standard deviation as follows:

$$\frac{\text{CFU}}{\text{mL}} = \frac{\text{Number of colonies} \times \text{Dilution factor}}{\text{Volume plated}} \quad (1)$$

Statistical Analysis: SPSS Statistics 26 software was used to evaluate the data's normal distribution and homogeneity of variance using Shapiro-Wilk and Levene's tests, respectively (IBM, New York, NY, USA). The values were expressed as the mean and one standard deviation. The statistical information was examined using one-way ANOVA. Tukey's range test was used to assess differences between the mean values. If p -values were <0.05 , results were considered statistically significant ($* p < 0.05$, $** p < 0.01$, and $*** p < 0.001$).

Proteins Extraction and Proteomic Analysis: To investigate the proteome of the yeast cells that were attached onto the surfaces being studied, liquid chromatography coupled to tandem mass spectrometry (LC-MS/MS)-based proteomic workflow was employed. The micro-pillar Ti and as-received surfaces in triplicate were incubated with the yeast strains as aforementioned. After incubation, the surfaces were gently washed to remove any loosely attached cells and transferred to 15 mL centrifuge tubes. The tubes were vortexed for 2 min and sonicated for 15 min to remove all of the attached cells. The surfaces were subsequently stained with calcofluor white and imaged under confocal to ensure no remaining cells. The cell suspension was transferred to a new tube for a further protein extraction process. At least three replicates per condition were conducted.

The cell suspension was mixed with an equal volume of 10% SDS in TEAB (100 mM) and 0.2 mm stainless steel beads (100 μL) (Next Advance, Troy, NY, USA). The samples were then subjected to homogenization using a bullet blender (Next Advance, Troy, NY, USA). Samples were spun at 13 000 rpm for 10 min, then the supernatant was transferred into a new tube. BCA assay (Thermo Fischer Scientific, San Jose, CA, U.S.A.) was used to measure the protein concentration. In the following steps, each replicated with same protein input underwent reduction, alkylation, and acidification processes at tris(2-carboxyethyl)phosphine (TCEP) (10 mM), iodoacetamide (IAA) (50 mM), and 2.5% phosphoric

acid (H_3PO_4), respectively. Samples were then mixed with a binding buffer (90% methanol/10% MilliQ water with 100 mM TEAB) and transferred into an S-trap micro (Protifi, USA) for the subsequent cleaning and digesting processes following the manufacturer's protocol. Trypsin (Thermo Fischer Scientific, USA) was used for overnight protein digestion at 37 °C. After incubation, peptides were eluted by a series of elution buffers, including TEAB (50 mM), 0.2% formic acid, and 50% acetonitrile (ACN), respectively. The eluted peptides were pooled and centrifuged using the SpeedVac concentrator (Thermo Fisher Scientific, San Jose, CA, USA) for the removal of acetonitrile before freeze drying. Dry peptides were resuspended in 2% ACN/ 0.05% trifluoroacetic acid (TFA) and loaded into the LC-MS/MS instrument for analysis.

The Nano-LC system, Ultimate 3000 RSLC (Thermo Fisher Scientific, San Jose, CA, USA) was set up with an Acclaim Pepmap RSLC analytical column (C18, 100 Å, 75 $\mu\text{m} \times 50$ cm, Thermo Fisher Scientific, San Jose, CA, USA) and Acclaim Pepmap nano-trap column (75 $\mu\text{m} \times 2$ cm, C18, 100 Å) and controlled at a temperature of 50 °C. Solvent A was 0.1% v/v formic acid and 5% v/v dimethyl sulfoxide (DMSO) in water and solvent B was 0.1% v/v formic acid and 5% DMSO in ACN. The trap column was loaded with tryptic peptide at an isocratic flow of 3% ACN containing 0.05% TFA at 6 $\mu\text{L min}^{-1}$ for 6 min, followed by the switch of the trap column as parallel to the analytical column. The gradient settings for the LC run, at a flow rate of 300 nL min^{-1} , were as follows: solvent B 3% to 4% in 1 min, 4% to 25% in 75 min, 25% to 40% in 4 min, 40% to 80% in 1 min, maintained at 80% for 3 min before dropping to 3% in 0.1 min and equilibration at 3% solvent B for 4.9 min.

Data-independent acquisition (DIA) was carried out on the Orbitrap Eclipse mass spectrometer (Thermo Fisher Scientific, San Jose, CA, USA). The settings of nanoelectrospray voltages, ion funnel RF, and capillary temperature were 1.9 kV, 30%, and 275 °C, respectively. A survey scan with an m/z range of 350 to 1400, a resolution of 120 000, an automatic gain control (AGC) target of $1e6$, a maximum ion trapping time of 50 ms was performed before 50 DIA windows with an m/z isolation window of 13.7, a precursor ion m/z range of 361–1033, an MS/MS scan range of m/z 200–2000, a resolution of 30 000, an AGC of $1e6$, a maximum ion trapping time of 55 ms and normalized collision energy (NCE) of 30%. Data was processed using Spectronaut 16.0 (Biognosys, Zurich, Switzerland) with direct DIA pipeline and the default BGS Factory settings. Trypsin as the enzyme, acetylation at the protein N-terminal and oxidation at methionine as variable modification, carbamidomethyl at cysteine as fixed modification, 1% false discovery rate (FDR) at PSM, peptide and protein levels were selected. The *C. albicans* and *C. auris* proteome databases from UniProt were downloaded for comparative analysis. Perseus 1.6.15.0 was used for unsupervised hierarchical clustering analysis (HCA) and two sample t-Test ($p < 0.05$ as well as $\log_2(\text{fold change}) > = 1$ or $< = -1$ were required for significance). The protein functional annotations were from UniProt.

Supporting Information

Supporting Information is available from the Wiley Online Library or from the author.

Acknowledgements

The authors would like to thank the ARC Research Hub for Australian Steel Manufacturing for funding this research. The authors would like to thank the Microscopy and Microanalysis Facility (RMMF) at RMIT University and the ARC Training Centre for Surface Engineering for Advanced Materials (SEAM) for the use of their facilities. This work was performed in part at the Melbourne Centre for Nanofabrication (MCN) in the Victorian Node of the Australian National Fabrication Facility (ANFF). The authors would like to thank the Melbourne Mass Spectrometry and Proteomics Facility at The Bio21 Molecular Science and Biotechnology Institute at The University of Melbourne. Graphical abstract was created with BioRender.com. This study was supported by the Australian Research Council through the ARC Research Hub for Australian Steel Manufacturing under the Industrial Transformation Research Hubs scheme (Project ID: IH130100017).

Open access publishing facilitated by RMIT University, as part of the Wiley - RMIT University agreement via the Council of Australian University Librarians.

Conflict of Interest

The authors declare no conflict of interest.

Author Contributions

P.H.L. and D.P.L. contributed equally to this work. E.P.I. designed the research; P.H.L., D.P.L., and A.A.M. performed the research; P.H.L., D.P.L., A.A.M., and S.N. analysed the data; P.H.L. and D.P.L. wrote the paper; E.P.I., S.N., N.A.W., R.J.C., and S.M. reviewed and edited the manuscript. All authors read and approved the manuscript.

Data Availability Statement

The data that support the findings of this study are available in the supplementary material of this article.

Keywords

antifungal properties, biomimetic surfaces, black titanium, *Candida albicans*, *Candida auris*, micropillars

Received: April 20, 2023

Revised: June 5, 2023

Published online: August 17, 2023

- [1] M. Kapitan, M. J. Niemiec, A. Steimle, J. S. Frick, I. D. Jacobsen, in *Fungal Physiology and Immunopathogenesis* (Ed.: M. L. Rodrigues), Springer International Publishing, Cham 2019.
- [2] M. A. Pfaller, D. R. Andes, D. J. Diekema, D. L. Horn, A. C. Reboli, C. Rotstein, B. Franks, N. E. Azie, *PLoS One* 2014, 9, 101510.
- [3] J. Guinea, *Clin Microbiol. Infect.* 2014, 20, 5.
- [4] M. Ademe, F. Girma, *Infect Drug Resist* 2020, 13, 1287.
- [5] S. Ahmad, W. Alfouzan, *Microorganisms* 2021, 9, 807.
- [6] O. Gudlaugsson, S. Gillespie, K. Lee, J. Vande Berg, J. Hu, S. Messer, L. Herwaldt, M. Pfaller, D. Diekema, *Clin. Infect. Dis.* 2003, 37, 1172.
- [7] A. Mombelli, F. Décaillot, *J. Clin. Periodontol.* 2011, 38, 203.
- [8] F. Schwarz, K. Becker, S. Rahn, A. Hegewald, K. Pfeffer, B. Henrich, *Int. J. Implant Dent* 2015, 1, 1.
- [9] I. Lafuente-Ibáñez de Mendoza, A. Cayero-Garay, G. Quindós-Andrés, J. M. Aguirre-Urizar, *Int. J. Implant Dent* 2021, 7, 1.
- [10] E. P. Ivanova, D. P. Linklater, A. A. Medina, P. Le, V. A. Baulin, H. Khuong Duy Nguyen, R. Curtain, E. Hanssen, G. Gervinskas, S. Hock Ng, V. Khanh Truong, P. Luque, G. Ramm, H. A. B. Wösten, R. J. Crawford, S. Juodkazis, S. Maclaughlin, *J. Colloid Interface Sci.* 2021, 603, 886.
- [11] D. P. Linklater, S. Juodkazis, S. Rubanov, E. P. Ivanova, *ACS Appl. Mater. Interfaces* 2017, 9, 29387.
- [12] E. P. Ivanova, J. Hasan, H. K. Webb, V. K. Truong, G. S. Watson, J. A. Watson, V. A. Baulin, S. Pogodin, J. Y. Wang, M. J. Tobin, C. Lötbe, R. J. Crawford, *Small* 2012, 8, 2489.
- [13] D. P. Linklater, V. A. Baulin, S. Juodkazis, R. J. Crawford, P. Stoodley, E. P. Ivanova, *Nat. Rev. Microbiol.* 2020, 19, 8.
- [14] E. P. Ivanova, J. Hasan, H. K. Webb, G. Gervinskas, S. Juodkazis, V. K. Truong, A. H. F. Wu, R. N. Lamb, V. A. Baulin, G. S. Watson, J. A. Watson, D. E. Mainwaring, R. J. Crawford, *Nat. Commun.* 2013, 4, 2838.

- [15] J. Hasan, R. J. Crawford, E. P. Ivanova, *Trends Biotechnol.* **2013**, *31*, 295.
- [16] D. P. Linklater, E. P. Ivanova, *Nano Today* **2022**, *43*, 101404.
- [17] J. Hasan, H. K. Webb, V. K. Truong, S. Pogodin, V. A. Baulin, G. S. Watson, J. A. Watson, R. J. Crawford, E. P. Ivanova, *Appl. Microbiol. Biotechnol.* **2013**, *97*, 9257.
- [18] S. Pogodin, J. Hasan, V. A. Baulin, H. K. Webb, V. K. Truong, T. H. Phong Nguyen, V. Boshkovikj, C. J. Fluke, G. S. Watson, J. A. Watson, R. J. Crawford, E. P. Ivanova, *Biophys. J.* **2013**, *104*, 835.
- [19] D. E. Mainwaring, S. H. Nguyen, H. Webb, T. Jakubov, M. Tobin, R. N. Lamb, A. H. Wu, R. Marchant, R. J. Crawford, E. P. Ivanova, *Nanoscale* **2016**, *8*, 6527.
- [20] V. K. Truong, N. M. Geeganagamage, V. A. Baulin, J. Vongsvivut, M. J. Tobin, P. Luque, R. J. Crawford, E. P. Ivanova, *Appl. Microbiol. Biotechnol.* **2017**, *101*, 4683.
- [21] S. Hawi, S. Goel, V. Kumar, O. Pearce, W. N. Ayre, E. P. Ivanova, *ACS Appl. Nano Mater* **2022**, *5*, 1.
- [22] D. P. Linklater, S. Juodkazis, R. J. Crawford, E. P. Ivanova, *Materialia* **2019**, *5*, 100197.
- [23] T. L. Clainche, D. Linklater, S. Wong, P. Le, S. Juodkazis, X. L. Guevel, J. L. Coll, E. P. Ivanova, V. Martel-Frchet, *ACS Appl. Mater. Interfaces* **2020**, *12*, 48272.
- [24] K. Nowlin, A. Boseman, A. Covell, D. LaJeunesse, *J. R. Soc. Interface* **2015**, *12*, 20140999.
- [25] N. V. Kollu, D. R. LaJeunesse, *ACS Omega* **2021**, *6*, 1361.
- [26] E. Beltrán-Partida, B. Valdez-Salas, M. Curiel-Álvarez, S. Castillo-Urbe, A. Escamilla, N. Nedev, *Mater. Sci. Eng. C* **2017**, *76*, 59.
- [27] A. Hayles, R. Bright, J. Wood, D. Palms, P. Zilm, T. Brown, D. Barker, K. Vasilev, *Adv. Mater. Interfaces* **2022**, *9*, 2102353.
- [28] C. Apip, A. Martínez, M. Meléndrez, M. Domínguez, T. Marzialetti, R. Báez, G. Sánchez-Sanhueza, A. Jaramillo, A. Catalán, *Saudi Dent. J.* **2021**, *33*, 944.
- [29] H. C. T. Firmino, E. P. Nascimento, R. F. Bonan, P. P. Maciel, L. R. C. Castellano, L. N. L. Santana, G. A. Neves, R. R. Menezes, *Mater. Lett.* **2021**, *283*, 128709.
- [30] S. V. Agarwalla, K. Ellepola, N. Silikas, A. H. Castro Neto, C. J. Seneviratne, V. Rosa, *Dent Mater* **2021**, *37*, 370.
- [31] Y. Yuan, Y. Zhang, *Nanomedicine* **2017**, *13*, 2199.
- [32] K. Leśniak-Ziółkowska, K. Brodac, D. Babilas, M. Dulski, A. Blacha-Grzechnik, X. Lu, A. Kazek-Kęsik, W. Simka, *Appl. Surf. Sci.* **2023**, *615*, 156285.
- [33] M. Mouhat, R. Moorehead, C. Murdoch, *Biomater. Investig. Dent.* **2020**, *7*, 146.
- [34] C. Aparicio, A. Padrós, F.-J. Gil, *J. Mech. Behav. Biomed. Mater.* **2011**, *4*, 1672.
- [35] J. G. S. Souza, R. C. Costa, A. A. Sampaio, V. L. Abdo, B. E. Nagay, N. Castro, B. Retamal-Valdes, J. A. Shibli, M. Feres, V. A. R. Barão, M. Bertolini, *iScience* **2022**, *25*, 103994.
- [36] F. Zeng, Y. Li, K. Chen, G. Li, C. Liu, L. Wang, L. Li, Q. Qu, *Bioelectrochemistry* **2022**, *148*, 108248.
- [37] A. Chakraborty, M. Jasieniak, B. R. Coad, H. J. Griesser, *ACS Appl. Bio Mater.* **2021**, *4*, 7769.
- [38] B. Valdez-Salas, E. Beltrán-Partida, M. Curiel-Álvarez, M. Guerra-Balcázar, N. Arjona, *ACS Omega* **2021**, *6*, 15625.
- [39] D. B. Roszak, R. R. Colwell, *Microbiol Rev* **1987**, *51*, 365.
- [40] P. H. Le, D. H. K. Nguyen, A. Aburto-Medina, D. P. Linklater, R. J. Crawford, S. MacLaughlin, E. P. Ivanova, *ACS Appl. BioMater.* **2020**, *3*, 8581.
- [41] J. T. Seil, T. J. Webster, *Int J Nanomedicine* **2012**, *7*, 2767.
- [42] H. Alalwan, C. J. Nile, R. Rajendran, R. McKerlie, P. Reynolds, N. Gadegaard, G. Ramage, *Nanomedicine* **2018**, *14*, 1045.
- [43] P. H. Le, D. H. K. Nguyen, A. A. Medina, D. P. Linklater, C. Loebbe, R. J. Crawford, S. MacLaughlin, E. P. Ivanova, *Nanomaterials* **2022**, *12*, 567.
- [44] J. Chandra, D. M. Kuhn, P. K. Mukherjee, L. L. Hoyer, T. McCormick, M. A. Ghannoum, *J. Bacteriol. Res.* **2001**, *183*, 5385.
- [45] G. G. S. M. Godoy, V. M. de Andrade, F. Dondeo, K. Conceição, A. Capella, *Mater. Chem. Phys.* **2023**, *294*, 127055.
- [46] J. G. Chiou, M. K. Balasubramanian, D. J. Lew, *Annu. Rev. Cell Dev. Biol.* **2017**, *33*, 77.
- [47] B. Aslam, M. Basit, M. A. Nisar, M. Khurshid, M. H. Rasool, *J. Chromatogr. Sci.* **2017**, *55*, 182.
- [48] C. Xie, Y. Jiang, Z. Zhu, S. Huang, W. Li, G. Ou, *Proc Natl Acad Sci USA* **2021**, *118*, 2100805118.
- [49] S. K. Maciver, P. J. Hussey, *Genome Biol.* **2002**, *3*, 12.
- [50] A. A. Petti, C. A. Crutchfield, J. D. Rabinowitz, D. Botstein, *Proc. Natl. Acad. Sci. USA* **2011**, *108*, E1089.
- [51] S. J. Singer, G. L. Nicolson, *Science* **1972**, *175*, 720.
- [52] I. Irminger-Finger, N. Mathis, *Cell Struct Funct* **1998**, *23*, 209.
- [53] A. Reinders, N. Burckert, T. Boller, A. Wiemken, C. De Virgilio, *Genes Dev.* **1998**, *12*, 2943.
- [54] L. Kraidlova, G. Van Zeebroeck, P. Van Dijck, H. Sychrova, *Eukaryot Cell* **2011**, *10*, 1219.
- [55] H. Chen, X. Zhou, B. Ren, L. Cheng, *Virulence* **2020**, *11*, 337.
- [56] M. Quick, J. A. Javitch, *Proc Natl Acad Sci U S A* **2007**, *104*, 3603.
- [57] B. Alberts, A. Johnson, J. Lewis, M. Raff, K. Roberts, P. Walter, in *Molecular Biology of the Cell*, 4th Ed, Garland Science, New York **2002**.
- [58] A. G. Hinnebusch, *Annu. Rev. Microbiol.* **2005**, *59*, 407.
- [59] D. J. Jamieson, *Yeast* **1998**, *14*, 1511.
- [60] J. Jenkins, J. Mantell, C. Neal, A. Gholinia, P. Verkade, A. H. Nobbs, B. Su, *Nat. Commun.* **2020**, *11*, 1626.
- [61] L. Rizzello, B. Sorce, S. Sabella, G. Vecchio, A. Galeone, V. Brunetti, R. Cingolani, P. P. Pompa, *ACS Nano* **2011**, *5*, 1865.
- [62] S. B. Park, C. S. Steadman, A. A. Chaudhari, S. R. Pillai, S. R. Singh, P. L. Ryan, S. T. Willard, J. M. Feugang, *J Nanobiotechnology* **2018**, *16*, 31.
- [63] D. Szklarczyk, A. L. Gable, K. C. Nastou, D. Lyon, R. Kirsch, S. Pyysalo, N. T. Doncheva, M. Legeay, T. Fang, P. Bork, L. J. Jensen, C. von Mering, *Nucleic Acids Res.* **2021**, *49*, D605.
- [64] F. Madeo, E. Herker, S. Wissing, H. Jungwirth, T. Eisenberg, K. U. Frohlich, *Curr. Opin. Microbiol.* **2004**, *7*, 655.
- [65] C. Mazzoni, E. Herker, V. Palermo, H. Jungwirth, T. Eisenberg, F. Madeo, C. Falcone, *EMBO Rep.* **2005**, *6*, 1076.
- [66] D. Carmona-Gutierrez, T. Eisenberg, S. Buttner, C. Meisinger, G. Kroemer, F. Madeo, *Cell Death Differ.* **2010**, *17*, 763.
- [67] R. Strich, *Genetics* **2015**, *200*, 1003.
- [68] S. Zhao, Z. Li, D. P. Linklater, L. Han, P. Jin, L. Wen, C. Chen, D. Xing, N. Ren, K. Sun, S. Juodkazis, E. P. Ivanova, L. Jiang, *Nano Lett.* **2022**, *22*, 1129.
- [69] C. Mazzoni, C. Falcone, *Biochim. Biophys. Acta* **2008**, *1783*, 1320.
- [70] S. R. Kushner, *IUBMB Life* **2004**, *56*, 585.
- [71] C. Mazzoni, P. Mancini, L. Verdona, F. Madeo, A. Serafini, E. Herker, C. Falcone, *Mol. Biol. Cell* **2003**, *14*, 721.
- [72] R. D. Silva, R. Sotoca, B. Johansson, P. Ludovico, F. Sansonetti, M. T. Silva, J. M. Peinado, M. Corte-Real, *Mol. Microbiol.* **2005**, *58*, 824.
- [73] H. Tabassum, S. Parvez, in *Epigenetics and Metabolomics*, Vol. 28 (Eds.: P. K. Agrawala, P. Rana), Academic Press, Cambridge, MA, USA **2021**.
- [74] H. K. Webb, V. K. Truong, J. Hasan, C. Fluke, R. J. Crawford, E. P. Ivanova, *Scanning* **2012**, *34*, 257.
- [75] E. P. Ivanova, V. K. Truong, J. Y. Wang, C. C. Berndt, R. T. Jones, I. I. Yusuf, I. Peake, H. W. Schmidt, C. Fluke, D. Barnes, R. J. Crawford, *Langmuir* **2010**, *26*, 1973.
- [76] N. David, K. Petr, *Open Phys* **2012**, *10*, 181.
- [77] D. P. Linklater, P. H. Le, A. Aburto-Medina, R. J. Crawford, S. MacLaughlin, S. Juodkazis, E. P. Ivanova, *Int. J. Mol. Sci.* **2023**, *24*, 1298.